Assessing Turbulent Models for Flow Accelerated Corrosion Prediction in a 90-Degree Bend

Phuris Khunphakdee[1,2], Ratchanon Piemjaiswang[3], Benjapon Chalermsinsuwan[4,*]

[1] Program of Petrochemistry and Polymer Science, Faculty of Science, Chulalongkorn University, 254 Phayathai Road, Wangmai, Pathumwan, Bangkok 10330, Thailand
[2] Boiler Department, Mechanical Maintenance Division, Electrical Generating Authority of Thailand (EGAT), 81 Moo 11, Bangkruai-Sainoi Road, Sainoi, Nonthaburi 11150, Thailand
[3] Environmental Research Institute, Chulalongkorn University, 254 Phayathai Road, Wangmai, Pathumwan, Bangkok 10330, Thailand
[4] Department of Chemical Technology, Faculty of Science, Chulalongkorn University, 254 Phayathai Road, Wangmai, Pathumwan, Bangkok 10330, Thailand

ARTICLE INFO	ABSTRACT
         Keywords: 	Flow accelerated corrosion (FAC), is still prevail in power plants piping components and is driven by variables in hydrodynamics, water chemistry and material composition groups. Amongst these factors, flow hydrodynamics play a major role as FAC is a corrosion process limited by wall mass transfer rates. Computational Fluid Dynamics (CFD) have been employed to calculate mass transfer coefficient for further FAC rate assessment. However, various turbulent models have been used in literatures. In this study, CFD calculations of mass transfer coefficient in 90-degree bend are performed with different turbulent models including $k-\varepsilon$ RNG, $k-\omega$ SST, Transition $k-kl-\omega$ and Transition SST at the Reynolds number (Re) of 90,000 and the Schmidt number (Sc) of 2.53. $k-\varepsilon$ RNG, Transition $k-kl-\omega$ and Transition SST models yield similar flow behaviour, while the $k-\omega$ SST shows the delay in the flow separation and double vortices development. The predicted mass transfer coefficients from the three models also agree with the experimental result. The $k-\varepsilon$ RNG outperforms the others with the maximum relative error of 14%. Although the obtained mass transfer coefficient from $k-\omega$ SST model shows good agreement with experimental results at the outlet part of the bend, high discrepancies exist at the inlet part.

1. Introduction

Flow accelerated corrosion or FAC damages have been recorded since 1972 as shown in the work of Gipon and Trevin [1]. Although preventive measures for Flow accelerated corrosion or FAC have been developed since 1986, the problems remain in many power plants nowadays. This indicates that a more thorough understanding of different aspects of the FAC is still needed.

FAC is a corrosion process starting from the magnetite layer formation through the Schikorr reaction, which takes place when reducing water is in contact with steel pipes' wall or component's

* *Corresponding author.*
E-mail address: benjapon.c@chula.ac.th

inner surface. Ferrous species from the component's wall at the wall-oxide interface then diffuses through the oxide layer. Meanwhile, ferrous species at the oxide-water interface of the magnetite layer are also dissolved to adjacent area. Finally, the diffused and dissolved species proceed to the bulk flow and convect downstream. The overall process can be described in Figure 1.
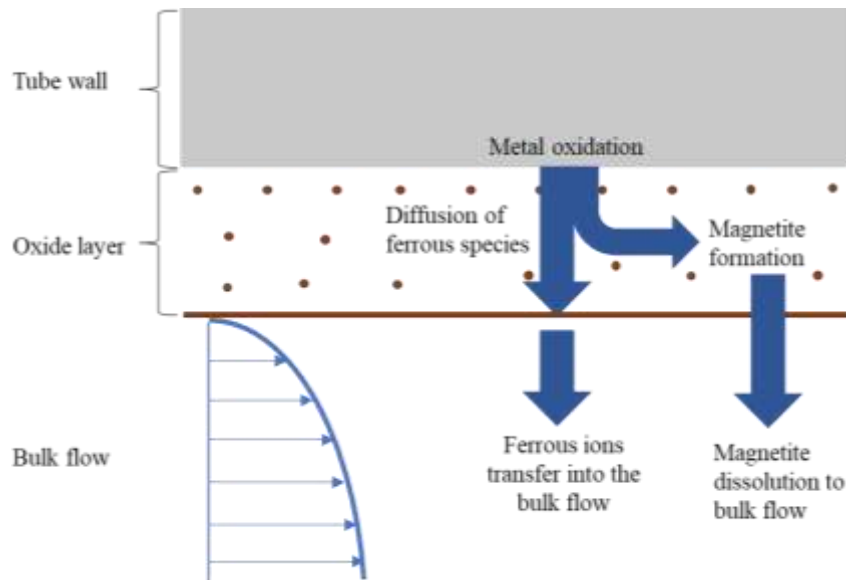
Fig. 1. Different steps in FAC [2]

FAC can be categorized into single-phase and two-phase FAC. For the former, water is in liquid phase and for the later, the water is a mixture between saturated liquid and saturated vapor. One of the iconic attributes of FAC is the horseshoe-like marks or the chevron-like marks on effected surfaces, as shown in Figure 2. Both the FAC are similar except that the two-phase FAC appears black and shinier compared to the single-phase FAC.

Fig. 2. Iconic horseshoe-like or chevron-like marks of FAC

Major FAC supported factors are from three major groups including hydrodynamics, water chemistry, and material composition. Many literature studies experimentally investigated the FAC rate on chemistry variables and material composition. For example, the cycle water pH value was found to affect the FAC rate and Dooley and Mathews [3] found that the FAC rate could be minimized by optimizing the pH level. Lotz and Postlethwaite [4] proved that high concentration corrosion inhibitors such as chromates and nitrites acted as passive inhibitors and could limit the FAC rate. Barth *et al.,* [5] reported that adding small amount of Chromium to carbon steel could effectively reduce the FAC.

Apart from the water chemistry and material composition, Mazhar [6] stated that flow hydrodynamics also played a major role as FAC was a corrosion process limited by wall mass transfer rates. The advancement of the computational fluid dynamics (CFD) codes and computational power allows numerical studies on fluid flow behavior and mass transfer, thus, FAC investigation. Developed mathematical models not only reproduce physical behaviors, but the obtained results also matched experimental results. This proves that CFD can be employed to analyze FAC effectively.

Various turbulent models are employed in different literatures and geometry. For example, El-Gammal *et al.,* [7] studied single-phase FAC in a 90-degree bend at the Reynolds number (RE) of 40,000. The Reynolds Stress Model (RSM) with standard wall function was employed. Correlations between the FAC damage locations and the turbulent flow parameters such as skin friction, turbulent kinetic energy and surface static pressure were also developed. The results agreed with the works of Nešić [8], Zinemanas and Herszage [9], and Poulson [10].

Another example of CFD study in FAC can be seen in the work from Lin and Ferng [11]. They examined the impacts of fluid dynamics on the FAC rate in a bend using enhanced wall treatment $k - \varepsilon$ RNG model. The flow behavior and mass transfer of oxygen from water to pipe wall were determined. Corrosion model from Keating and Nešić [12] and the correlation between the dilution-diffusion coefficient presented by Hayduk and Minhas [13] were employed.

A similar single-phase FAC study was done by Prasad *et al.,* [14] using $k - \varepsilon$ RNG turbulent model. The correlation adopted from Pietralik [15] was applied in the calculation of mass transfer coefficient (MTC). This MTC included the geometrical effect and the time-changing wall roughness. The applications to flow in a 58° bend and in a straight pipe downstream an orifice showed promising results.

As there is no literature that compares results obtained from different models with the same geometry, hence, in this study, mass transfer coefficients, in 90-degree bend are studied using CFD with different turbulent models and wall models. The testing geometry, the relevant theories as well as the studied cases are provided in the methodology section. Then, the comparisons of the results from each case are shown and the advantages and disadvantages of different models are finally discussed.

2. Methodology
2.1 Problem Description

The problem to be studied in this study is flow of air in a naphthalene-coated 90° bend, the summary of which can be seen in Figure 3. Naphthalene-air system is chosen because the system is widely used in experiments and the mass transfer is considered low mass flux which is also the case for transportation of iron species from component wall to water in power plant piping system. This is done in Ansys Fluent. The domain of the problem is 90° bend with upstream and downstream pipes which is divided into 5 parts, the inlet straight pipe, the straight pipe upstream of the bend, the bend, the straight pipe downstream of the bend, and the outlet straight pipe. The pipe has a diameter of

0.07 m, and the bend radius is 1.5 times the pipe diameter. The length of the inlet and outlet of the straight pipes is defined such that the flow is fully developed. In addition, the analysis is three dimensional.
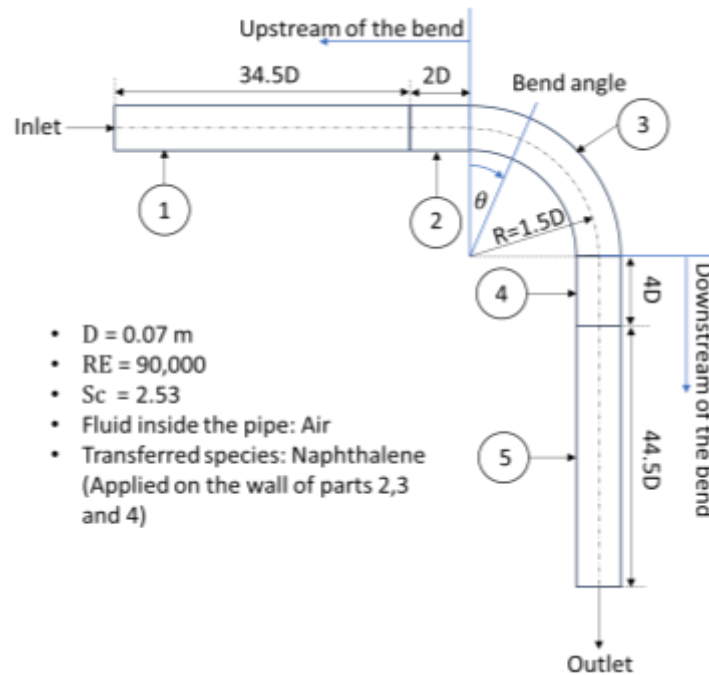
Fig. 3. Problem description the the calculation domain

The Reynolds number for this model is 90,000 and the Schmidt number is 2.53, which is the condition experimentally studied by Achenbach [16]. For near wall studies of fluid flow, it is suggested that the y^+ is kept below 5 in the work of Cebeci [17] and Luchini [18] to use viscous sublayer wall function with minimal deviations from the universal velocity profile close to the wall. Because mass transfer phenomenon requires determination of concentration gradients on the wall and the mass transfer boundary layer thickness is connected to the momentum boundary layer thickness by the factor of $Sc^{1/3}$, hence, the grid is generated such that the y^+ is kept below 3.5. Grid generation is done on Fluent meshing. The minimum and maximum sizes of the surface meshing are 0.0006 and 0.0008 m, respectively. The surface meshing growth rate is 1.4. Three layers of boundary mesh are added with the transition ratio of 0.272 with the same growth rate as the surface meshing. For the element meshing, the type of polyhedral is chosen as this is a balancing choice for accuracy, flexibility and computational cost as studied in the work of Wang *et al.,* [19]. The growth rate is also 1.4 and the maximum element size is approximately 0.001 m. The total number of cells after grid independent study is 32 million and the minimum orthogonal is 0.2. The experimental results from Achenbach [16] are used to validate the mass transfer coefficient obtained from CFD models. The boundary condition for the inlet is uniformed inlet velocity. For the outlet, the boundary condition is pressure outlet and for the walls of part 1-5 is assigned as no-slip wall. In addition, to study the mass transfer behavior, the wall of the part 1-3 is also assigned Naphthalene mass concentration of one.

2.2 Turbulent Flow Models

Turbulent flow has irregularities and random nature as its distinguished characters. Such complex flow can be solved by different strategies like Direct Numerical Simulation (DNS), Large Eddy Simulation (LES), and Reynolds Averaged Navier-Stokes (RANS). DNS and LES are usually used for

research purposes as well as for RANS models development. These strategies are not practical for industrial purposes because they require a great amount of computational resources as the former solves the Navier-Stokes equations at all length and time scales and while the later solves for the large and intermediate length and time scales. The RANS strategy is widely used in industries because of its affordable requirement in computational power. This technique solves a turbulent model that developed to resolve the closure problem by the emerging Reynold stress terms.

The RANS can be written as in the Eq. (1) and Eq. (2).

$$\nabla \cdot \vec{\overline{U}} = 0 \tag{1}$$

$$\rho \left[\frac{\partial \vec{\overline{U}}}{\partial t} + \vec{\overline{U}} \cdot \nabla \vec{\overline{U}} \right] = -\nabla \bar{p} + \mu \nabla^2 \vec{\overline{U}} - \rho \frac{\partial (\overline{u_i' u_j'})}{\partial x_j} \tag{2}$$

where μ is the dynamic viscosity of the fluid, $\bar{p}$ and $\vec{\overline{U}}$ are the mean pressure and mean velocity, and u_i' is the velocity fluctuation in the i direction. The last term in the Eq. (2) is called the Reynolds stress which are models in RANS turbulent models to resolve the closure problem.

The turbulent models studied in this research include $k - \varepsilon$ RNG, $k - \omega$ SST, Transition $k - kl - \omega$, and Transition $-$ SST models. The $k - \varepsilon$ RNG model, two-equation eddy-viscosity model, is developed by Yakhot *et al.,* [20] which renormalizes the Navier-Stokes equations using Re-Normalisation Group (RNG) methods. The purpose of this model development is to include the effects of smaller scales of motion to the turbulent diffusion which originally takes the effect of the specified scale in the $k - \varepsilon$ model. The $k - \omega$ SST turbulence model developed by Menter [21] is also a two-equation eddy-viscosity model combining the advantages of the $k - \omega$ model which perform better in the inner parts of the boundary layer due to no damping effects and k-ε which perform well in the area without adverse pressure gradient. The transition $k - kl - \omega$ model is a three-equation eddy-viscosity developed by Walters and Cokljat [22] to predict boundary layer development and calculate transition beginning point. In addition, the model can also be used to handle the transition of laminar to turbulent boundary effectively. Finally, the transition SST model combines the $k - \omega$ SST transport equations with two additional transport equations to handle the intermittency and the onset of transition based on the momentum-thickness Reynolds number.

2.3 Mass Transfer Model

The governing equations for fluid flow and mass transfer can be decoupled as the concentration of the species from the corrosion reaction is dilute, the reactions on the wall does not significantly affect the flow [23]. As stated earlier, FAC is limited by wall mass transfer rate. The mass transfer mechanism involves mass diffusion from wall to the bulk flow and mass convection that brings the diffused species downstream. The transport equation of chemical species, Y_i, implemented in Ansys Fluent can be written in the general form as in Eq. (3).

$$\frac{\partial (\rho Y_i)}{\partial t} + \nabla \cdot (\rho \vec{v} Y_i) = -\nabla \cdot \vec{J_i} + R_i + S_i \tag{3}$$

where Y_i is the mass fraction of the transported species, which is Naphthalene in this case, $\vec{v}$ is the fluid velocity. The first term is the rate of change of the mass fraction with time. The second and third terms are the mass transport by convection and diffusion, respectively. R_i and S_i, which are disabled,

represent the rate of species production by chemical reaction and the rate at which a species is generated through addition from the dispersed phase, as well as any user-defined sources.

2.4 Wall Sherwood Number Determination

In mass transfer calculation, ratios of the Sherwood number (Sh) at the bend wall to that of the fully developed flow in pipe (Sh_p) with identical diameter are evaluated. The expression for the Sh_p can be found in literatures or, for low mass flux conditions, by substituting the Nusselt and Prandtl numbers with the Sherwood and Schmidt numbers in an appropriate expression of heat transfer coefficient. In this study, the expression used in the work of Asadi and Esfahany [24] is taken and can be written as in Eq. (4).

$$Sh_p = 0.023Re^{0.8}Sc^{1/3} \tag{4}$$

The mass convection coefficient of the bend wall at different locations can be determined by balancing the mass diffusion from wall and the mass convection to the bulk flow as in the Eq. (5).

$$h_{mass} = \frac{-D\left(\frac{\partial Y_i}{\partial \bar{n}}\right)_w}{Y_{i,w}-Y_{i,avg}} \tag{5}$$

where $\left(\frac{\partial Y_i}{\partial \bar{n}}\right)_w$ is the wall mass fraction gradient in the direction normal to the wall, $Y_{i,w}$ is the mass fraction at the wall and $Y_{i,avg}$ is the average mass fraction on the cross-sectional area at the location.

Once the mass convection coefficient is known, the Sherwood number can be evaluated from the Eq. (6).

$$Sh = \frac{h_{mass}L}{D} \tag{6}$$

where L is the characteristic length of the problem and D is the mass diffusion coefficient which can be determined from the Sc.

3. Results and Discussion
3.1 Pressure Distribution

Figure 4 shows the contour of the pressure obtained from the calculations. Qualitatively, the pressure is low at the bend intrados wall due to the flow acceleration and separation, which is similar to the results obtained by Kumar *et al.,* [25]. On the other hand, the pressure is high at the bend extrados wall due to the flow deceleration. The $k-\varepsilon$ RNG and Transition $k-kl-\omega$ and Transition SST models could capture the lowest pressure zone at the beginning of the intrados while this is not clearly seen in the result from $k-\omega$ SST. This may be due to the fact that, at the zone close to the wall, the $k-\omega$ SST switches to $k-\omega$ model which could underperform the $k-\varepsilon$ RNG and other models in this particular zone.
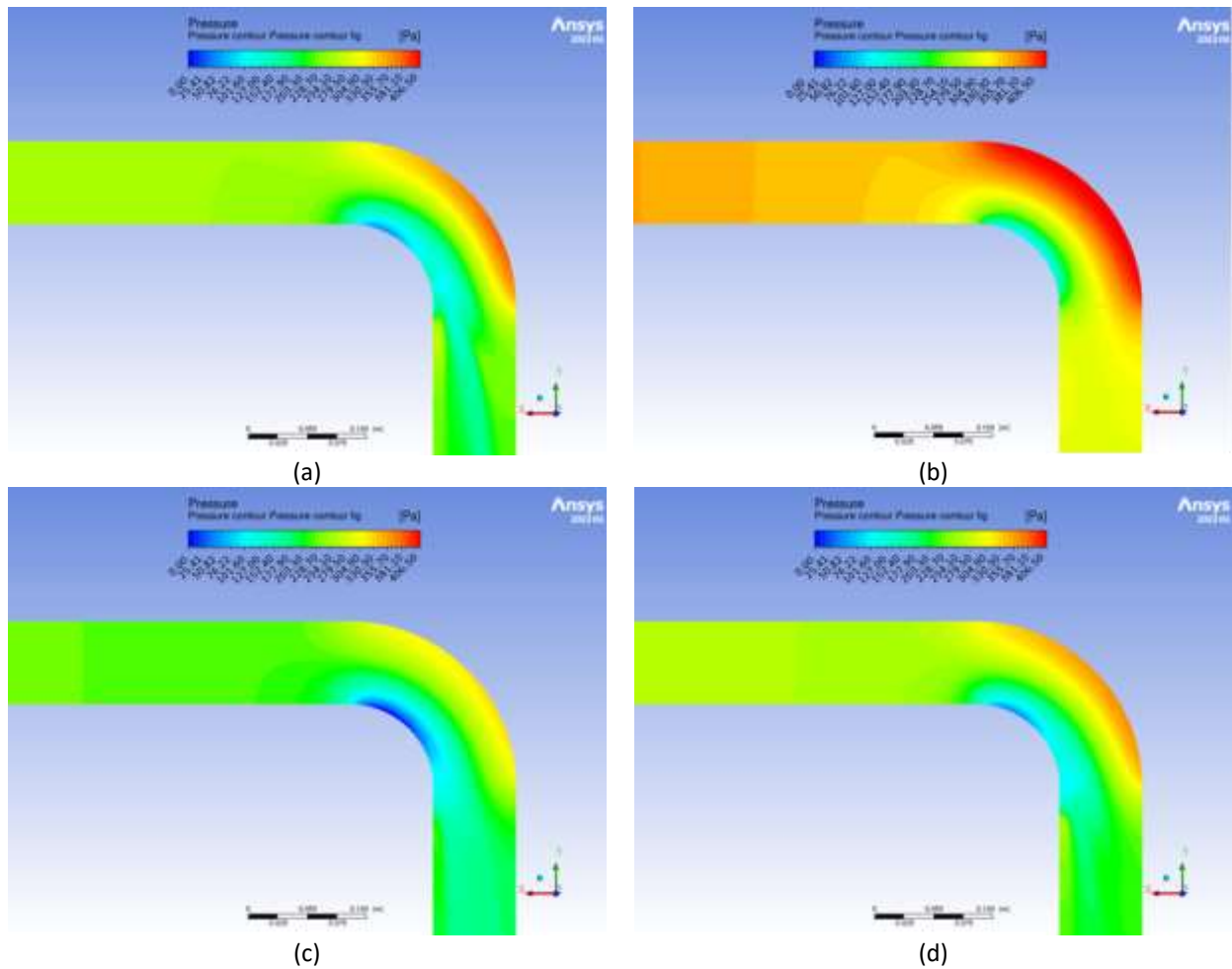
Fig. 4. Pressure contour (a) from $k - \varepsilon$ RNG model, (b) from $k - \omega$ SST model, (c) from Transition $k - kl - \omega$ model and (d) from Transition $-$ SST model

3.2 Velocity Distribution

The contour of the velocity magnitude can be seen in the Figure 5. The acceleration of the flow can be seen at the inlet of the bend intrados, where the pressure is minimum. The air is flowing into the bend inlet and is impinging on the extrados wall. Flow separation can be seen on the intrados near the exit of the elbow. This behaviour can be seen from the results of all models however, the starting point of the flow separation from $k - \omega$ SST comes later compared to the others.
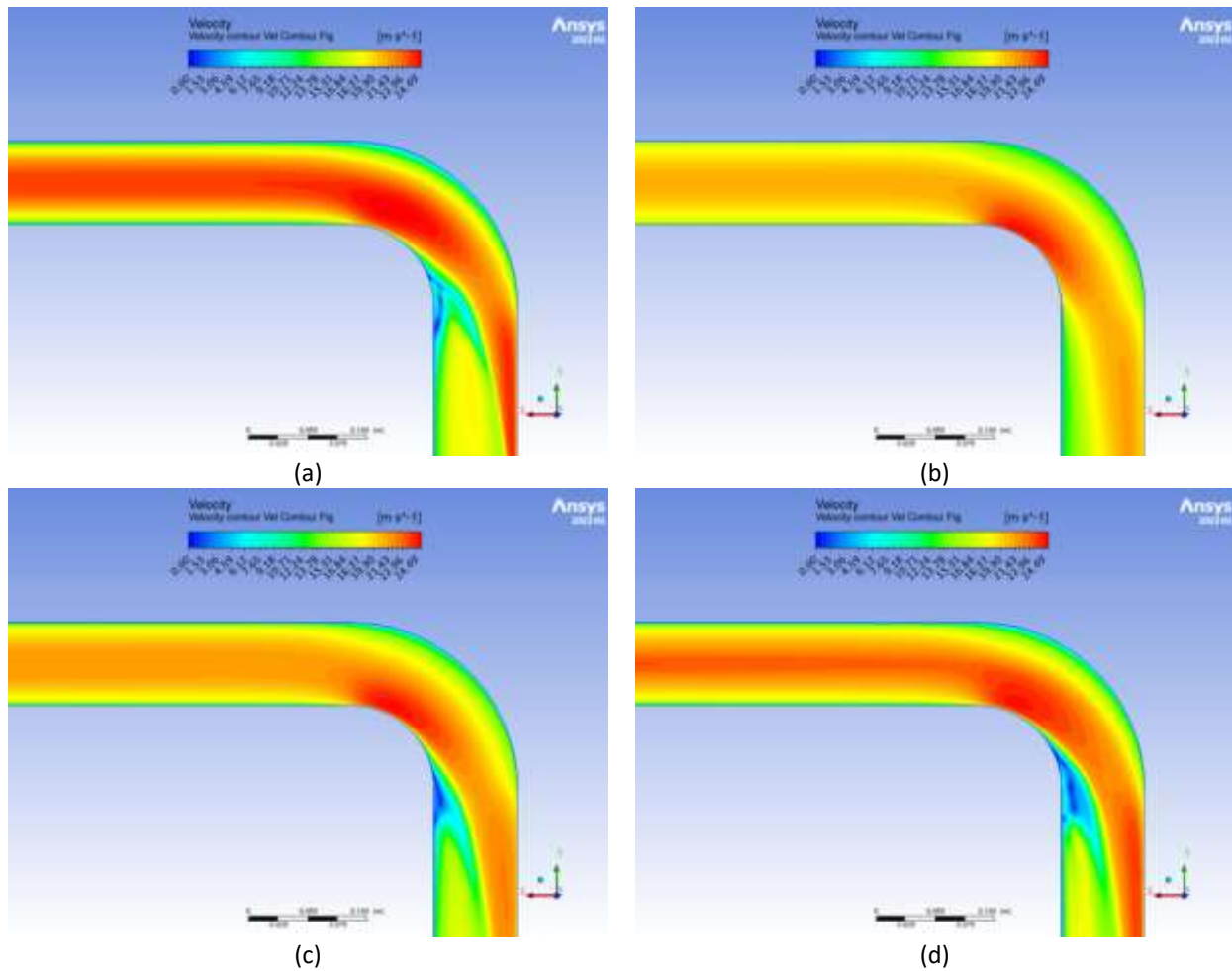
Fig. 5. Velocity magnitude contour (a) from $k - \varepsilon$ RNG model, (b) from $k - \omega$ SST model, (c) from Transition $k - kl - \omega$ model and (d) from Transition $-$ SST model

3.3 Velocity Vector at 20-Degree Plane

The velocity vector at the bend 20-degree plane is presented in the Figure 6. In the figure, the development of the double vortices can be seen. The air is flow from the intrados side (bottom part of each figure) to the extrados side (top part of each figure) and then goes along the sides wall back to the intrados. The result from $k - \varepsilon$ RNG model shows the strongest development judging by the magnitude of the velocity, followed by the Transition $k - kl - \omega$ and Transition SST. The $k - \omega$ SST model portrays this behavior the weakest.
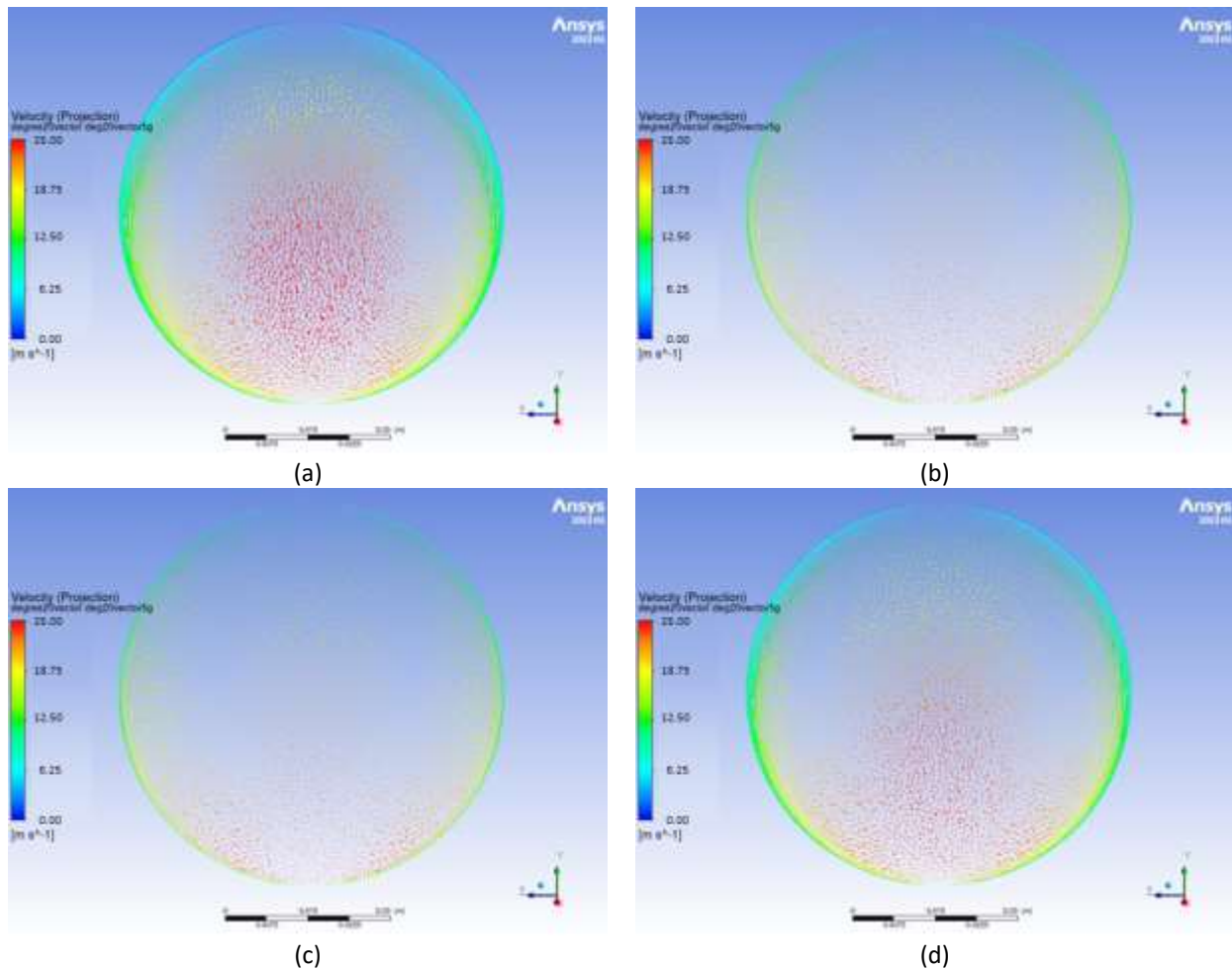
Fig. 6. Velocity vector on the bend 20-degree plane (a) from $k - \varepsilon$ RNG model, (b) from $k - \omega$ SST model, (c) from Transition $k - kl - \omega$ model and (d) from Transition $-$ SST model

3.4 Velocity Vector at 90-Degree Plane

As the flow progresses toward the bend outlet, the vortices can be clearly seen as shown in the Figure 7. The velocity vector at the outlet plane where the intrados and extrados are on the left and right side of each figure, respectively. On this outlet plane, the flow separation and the recirculation zones can be distinctively seen. $k - \varepsilon$ RNG and Transition SST models display qualitatively comparable results. The result from Transition $k - kl - \omega$ model agree with the formers. However, the result from the $k - \omega$ SST model does not show the flow separation yet and the vortices cannot be seen clearly as can be seen from the others.
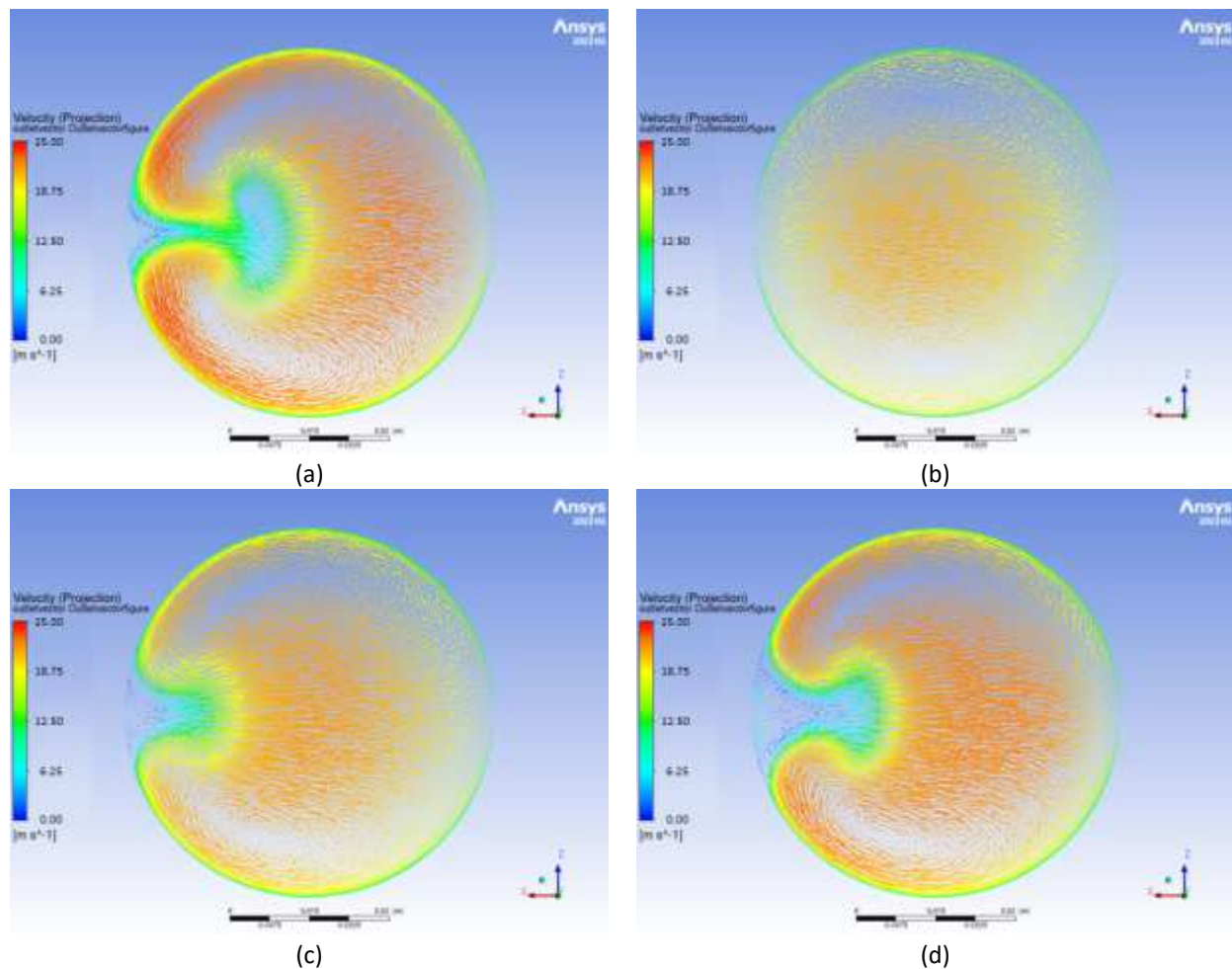
Fig. 7. Velocity vector on the bend outlet plane (a) from $k - \varepsilon$ RNG model, (b) from $k - \omega$ SST model, (c) from Transition $k - kl - \omega$ model and (d) from Transition $-$ SST model

3.5 Mass Transfer Coefficient on the Bend Extrados Wall

The ratios of the bend extrados Sherwood number to the straight pipe Sherwood number obtained from different turbulent models are shown in the Figure 8 together with the experimental data from Achenbach [16]. From the data, the Sherwood number of the bend extrados is approximately one near the bend inlet and is increasing as the flow progresses through the bend until reaching the bend outlet. This behavior is likely because of the impingement of the high velocity core flow, from the double vortices, onto the outer wall which causes high static pressure at the bend wall [6].
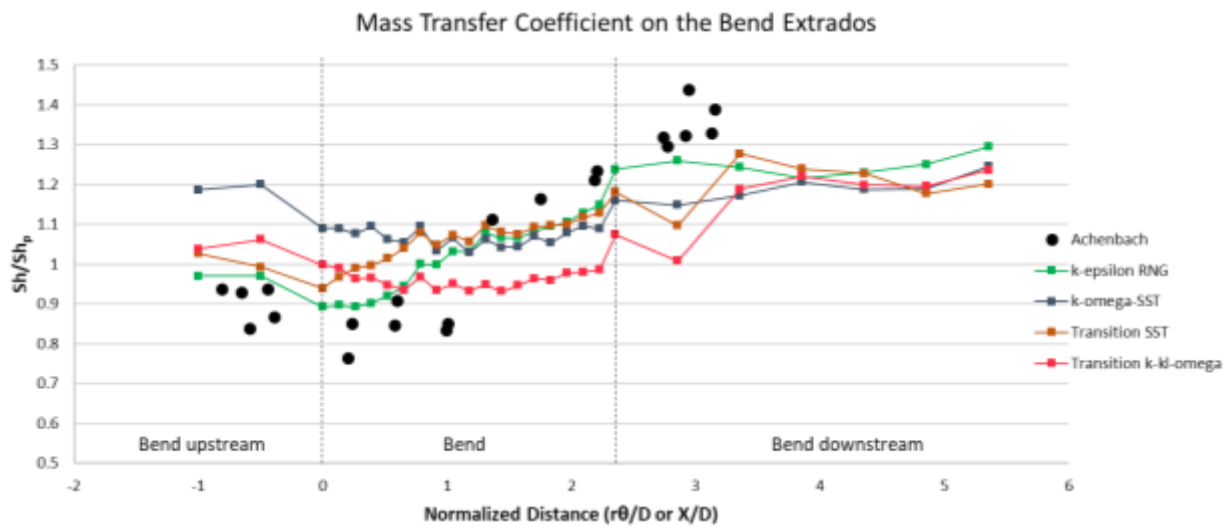
Fig. 8. Mass transfer coefficient ratio on the bend extrados wall

From the Figure 8, the $k - \varepsilon$ RNG gives the best matching result with the experimental data with the maximum relative error of 14%. It reflects both the inlet and outlet ends mass transfer behaviour correctly. The Transition $k - kl - \omega$, and Transition $-$ SST models give good agreement results compared to the benchmark data, at the maximum relative error about 17% and 22.5%, respectively, however, the slope of the curves in the bend section is less than the result by the $k - \varepsilon$ RNG. Finally, the $k - \omega$ SST model gives the same trend as the experimental data at the bend outlet and the downstream of the bend, but there is high discrepancy at the upstream and front half of the bend, the maximum relative error obtained from this model is as high as 25%.

Knowing that the $k - \omega$ SST employs $k - \omega$ model near the wall and $k - \varepsilon$ model away from the wall, Shahid and Agelin-Chaab [26], further investigation have been done by perform the calculation using the $k - \varepsilon$ model. The velocity vector plots at the outlet plane from the $k - \omega$ SST, $k - \varepsilon$, and $k - \varepsilon$ RNG are shown in the Figure 9 below. The solutions from $k - \omega$ SST and $k - \varepsilon$ are qualitatively the same while the solution from $k - \varepsilon$ RNG is distinct from the others.

(a)   (b)

(c)
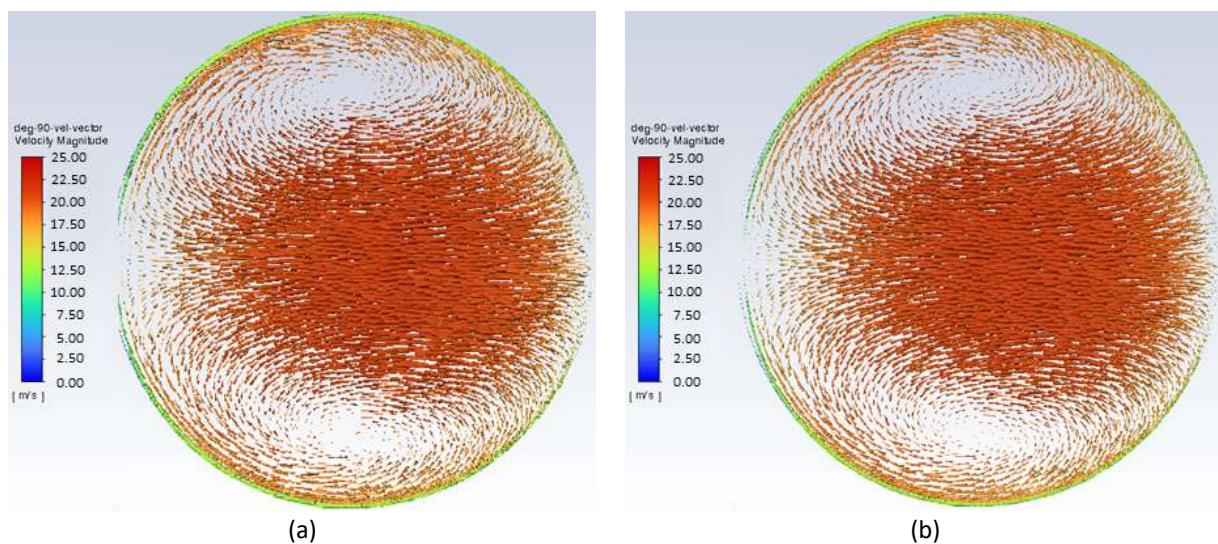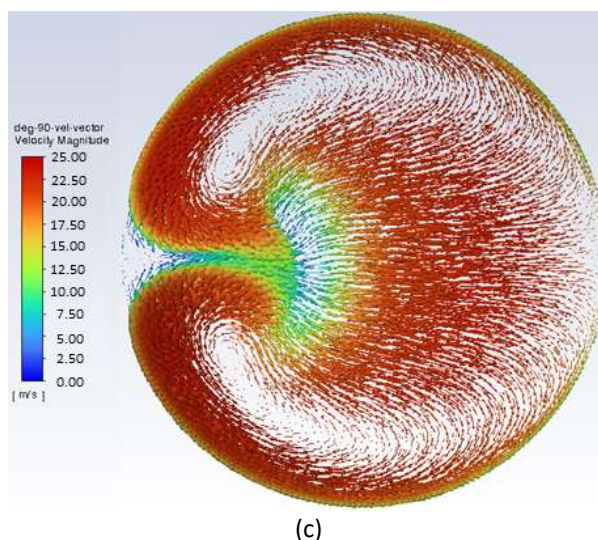
Fig. 9. Velocity vector on the bend outlet plane (a) from $k - \omega$ SST model, (b) from $k - \varepsilon$ model, and (c) from $k - \varepsilon$ RNG model

4. Conclusion

Turbulent flow in 90-degree bend has its own characteristics such as the flow separation and the secondary vortices resulting from the centrifugal effects as investigated in the work of Fiedler [27]. From the results, all models can capture these characters quite well. The $k - \varepsilon$ RNG, Transition $k - kl - \omega$, and Transition $-$ SST give comparable results to each other while the result from $k - \omega$ SST shows the delay of the flow separation starting point and the double vortices development. This may contribute to the fact that the $k - \varepsilon$ RNG models already account for the effects of smaller scales of motion and the Transition $k - kl - \omega$ and Transition $-$ SST models have been modified such that the complexities in the boundary layer can be taken care of.

Mass transfer analysis requires finer mesh near the wall as its boundary layer is usually thinner compared to the momentum boundary layer. In addition, as the velocity is almost zero near the wall, this requires low Reynolds number treatment in the turbulent model. For the studied problem, the $k - \varepsilon$ RNG model gives the most accurate results amongst the others. It can capture the ratio of the Sherwood number correctly both on the inlet and outlet side of the bend while the $k - \omega$ SST gives good agreement result at the outlet of the bend but shows large deviation at the inlet.

The reason of large discrepancies in the $k - \omega$ SST may arise from the usage of the $k - \varepsilon$ model instead of $k - \varepsilon$ RNG model in the regions away from the wall, Liu *et al.,* [28]. The better results from $k - \varepsilon$ RNG over the normal $k - \varepsilon$ model may come from the improvements in different aspects such as the effective viscosity modelling, the modification of the calculated effective viscosity to account for the swirl or rotation effects and the improved response to flows with rapid strained and streamline curvature by the additional R_ϵ term in the ε equation, referred to the work of Li *et al.,* [29] for the full equation.

From the findings, the $k - \varepsilon$ RNG model can be applied to study FAC in bends and in other complex geometries that are expected to have flow separation and vortices.

References

[1]   Gipon, Elodie, and Stéphane Trevin. "Flow-accelerated corrosion in nuclear power plants." In *Nuclear Corrosion*, pp. 213-250. Woodhead Publishing, 2020. https://doi.org/10.1016/B978-0-12-823719-9.00006-8

[2]   Khunphakdee, Phuris, and Benjapon Chalermsinsuwan. "Review of flow accelerated corrosion mechanism, numerical analysis, and control measures." *Chemical Engineering Research and Design* 197 (2023): 519-535. https://doi.org/10.1016/j.cherd.2023.08.012

[3]   Dooley, R. B., and J. Mathews. "The current state of cycle chemistry for fossil plants." In *Fifth International Cycle Chemistry Conference*. EPRI TR-108469. 1997.

[4]   Lotz, U., and J. Postlethwaite. "Erosion-corrosion in disturbed two phase liquid/particle flow." *Corrosion Science* 30, no. 1 (1990): 95-106. https://doi.org/10.1016/0010-938X(90)90239-2

[5]   Barth, Andy, Harold M. Crockett, Lee F. Goyette, Jeffrey S. Horowitz, and Robert Montgomery. "Flow Accelerated Corrosion: The Entrance Effect." In *ASME Pressure Vessels and Piping Conference*, vol. 48296, pp. 873-882. 2008. https://doi.org/10.1115/PVP2008-61185

[6]   Mazhar, Hazem. "Flow Accelerated Corrosion in Single and Dual S-Shape Bends under Single and Two Phase Annular Flow Conditions." *PhD diss., McMaster University*, 2014.

[7]   El-Gammal, Moustafa, H. Mazhar, J. S. Cotton, C. Shefski, John Pietralik, and C. Y. Ching. "The hydrodynamic effects of single-phase flow on flow accelerated corrosion in a 90-degree elbow." *Nuclear Engineering and Design* 240, no. 6 (2010): 1589-1598. https://doi.org/10.1016/j.nucengdes.2009.12.005

[8]   Nešić, Srdjan. "Using computational fluid dynamics in combating erosion-corrosion." *Chemical Engineering Science* 61, no. 12 (2006): 4086-4097. https://doi.org/10.1016/j.ces.2006.01.052

[9]   Zinemanas, Daniel, and A. Herszage. "Flow accelerated corrosion: flow field and mass transport in bifurcations and nozzles." In *15th International Conference on the Properties of Water and Steam*, Berlin, Germany. 2008.

[10] Poulson, Bryan. "Complexities in predicting erosion corrosion." *Wear* 233 (1999): 497-504. https://doi.org/10.1016/S0043-1648(99)00235-5

[11] Lin, Chih Hung, and Yuh Ming Ferng. "Predictions of hydrodynamic characteristics and corrosion rates using CFD in the piping systems of pressurized-water reactor power plant." *Annals of Nuclear Energy* 65 (2014): 214-222. https://doi.org/10.1016/j.anucene.2013.11.007

[12] Keating, A., and S. Nešić. "Numerical Prediction of Erosion-Corrosion in Bends." *Corrosion* 57, no. 7 (2001): 621-633. https://doi.org/10.5006/1.3290389

[13] Hayduk, W., and B. S. Minhas. "Correlations for prediction of molecular diffusivities in liquids." *The Canadian Journal of Chemical Engineering* 60, no. 2 (1982): 295-299. https://doi.org/10.1002/cjce.5450600213

[14] Prasad, Mahendra, V. Gopika, Arunkumar Sridharan, and Smrutiranjan Parida. "Pipe wall thickness prediction with CFD based mass transfer coefficient and degradation feedback for flow accelerated corrosion." *Progress in Nuclear Energy* 107 (2018): 205-214. https://doi.org/10.1016/j.pnucene.2018.04.024

[15] Pietralik, John M. "The role of flow in flow-accelerated corrosion under nuclear power plant conditions." *Japan Society of Maintenology, E-Journal of Advanced Maintenance* 4, no. 2 (2012): 63-78.

[16] Achenbach, Elmar. "Mass transfer from bend of circular cross section to air." *Future Energy Production Systems* 1 (1976): 327-227.

[17] Cebeci, T. "General behavior of turbulent boundary layers." *Analysis of Turbulent Flows with Computer Programs* (2013): 89-153. https://doi.org/10.1016/B978-0-08-098335-6.00004-5

[18] Luchini, Paolo. "Structure and interpolation of the turbulent velocity profile in parallel flow." *European Journal of Mechanics-B/Fluids* 71 (2018): 15-34. https://doi.org/10.1016/j.euromechflu.2018.03.006

[19] Wang, Wei, Yong Cao, and Tsubasa Okaze. "Comparison of hexahedral, tetrahedral and polyhedral cells for reproducing the wind field around an isolated building by LES." *Building and Environment* 195 (2021): 107717. https://doi.org/10.1016/j.buildenv.2021.107717

[20] Yakhot, V., Steven A. Orszag, Siva Thangam, T. B. Gatski, and C. G. Speziale. "Development of turbulence models for shear flows by a double expansion technique." *Physics of Fluids A: Fluid Dynamics* 4, no. 7 (1992): 1510-1520. https://doi.org/10.1063/1.858424

[21] Menter, Florian R. "Two-equation eddy-viscosity turbulence models for engineering applications." *AIAA Journal* 32, no. 8 (1994): 1598-1605. https://doi.org/10.2514/3.12149

[22] Walters, D. Keith, and Davor Cokljat. "A three-equation eddy-viscosity model for Reynolds-averaged Navier-Stokes simulations of transitional flow." *Journal of Fluids Engineering* 130, no. 12 (2008): 121401. https://doi.org/10.1115/1.2979230

[23] Wang, Jianrong, and Siamack A. Shirazi. "A CFD based correlation for mass transfer coefficient in elbows." *International Journal of Heat and Mass Transfer* 44, no. 9 (2001): 1817-1822. https://doi.org/10.1016/S0017-9310(00)00222-2

[24] Asadi, Tahereh, and Mohsen Nasr Esfahany. "Numerical Investigation of Turbulent Mass Transfer in a 90° Bend." *Iranian Journal of Chemistry and Chemical Engineering (IJCCE)* 34, no. 4 (2015): 113-121.

[25] Kumar, Shivam, Mukund Kumar, Samiran Samanta, Manoj Ukamanal, Asisha Ranjan Pradhan, and Shashi Bhushan Prasad. "Simulations of water flow in a horizontal and 90^0 pipe bend." *Materials Today: Proceedings* 56 (2022): 889-895. https://doi.org/10.1016/j.matpr.2022.02.528

[26] Shahid, Seham, and Martin Agelin-Chaab. "Battery thermal management through simulation and experiment: Air cooling and enhancement." In *Handbook of Thermal Management Systems*, pp. 221-254. Elsevier, 2023. https://doi.org/10.1016/B978-0-443-19017-9.00008-8

[27] Fiedler, H. E. "A note on secondary flow in bends and bend combinations." *Experiments in Fluids* 23, no. 3 (1997): 262-264. https://doi.org/10.1007/s003480050109

[28] Liu, Shengnan, Muk Chen Ong, Charlotte Obhrai, Inno Gatin, and Vuko Vukčević. "Influences of free surface jump conditions and different k– ω SST turbulence models on breaking wave modelling." *Ocean Engineering* 217 (2020): 107746. https://doi.org/10.1016/j.oceaneng.2020.107746

[29] Li, Jun-Sen, Li-Tao Zhu, Wei-Cheng Yan, Taha Abbas Bin Rashid, Qun-Jie Xu, and Zheng-Hong Luo. "Coarse-grid simulations of full-loop gas-solid flows using a hybrid drag model: Investigations on turbulence models." *Powder Technology* 379 (2021): 108-126. https://doi.org/10.1016/j.powtec.2020.10.052